Journal of Nuclear Materials 477 (2016) 42–49

Contents lists available at ScienceDirect

Journal of Nuclear Materials

journal homepage: www.elsevier.com/locate/jnucmat

Effect of rhenium irradiations on the mechanical properties of tungsten for nuclear fusion applications

Aneeqa Khan [a, *], Robert Elliman [b], Cormac Corr [b], Joven J.H. Lim [c], Andrew Forrest [c], Paul Mummery [a], Llion M. Evans [d]

[a] School of Mechanical, Aerospace and Civil Engineering, The University of Manchester, M13 9PL, UK
[b] Research School of Physics and Engineering, The Australian National University, Canberra, ACT 2601, Australia
[c] School of Materials, The University of Manchester, M13 9PL, UK
[d] Culham Centre for Fusion Energy, Culham Science Centre, Abingdon, Oxon, OX14 3DB, UK

ARTICLE INFO

Article history:
Received 22 February 2016
Received in revised form
26 April 2016
Accepted 2 May 2016
Available online 3 May 2016

ABSTRACT

As-received and annealed tungsten samples were irradiated at a temperature of 400 °C with Re and W ions to peak concentrations of 1600 appm (atomic parts per million) and damage levels of 40 dpa (displacements per atom). Mechanical properties were investigated using nanoindentation, and the orientation and depth dependence of irradiation damage was investigated using Electron Back Scatter Diffraction (EBSD). Following irradiation there was a 13% increase in hardness in the as received sheet and a 23% increase in the annealed material for both tungsten and rhenium irradiation. The difference between the tungsten and rhenium irradiated samples was negligible, suggesting that for the concentrations and damage levels employed, the presence of rhenium does not have a significant effect on the hardening mechanism. Energy dependent EBSD of annealed samples provided information about the depth distribution of the radiation damage in individual tungsten grains and confirmed that the radiation damage is orientation dependant.

1. Introduction

Tungsten is a candidate material for the divertor in future fusion reactors [1], due to its high melting point of 3420 °C [2], low sputtering rate [3] and its strength at high temperatures [4]. During the D-T operation of ITER and DEMO, 14 MeV neutrons will cause irradiation damage, including displacement cascades and transmutation of the tungsten. This is expected to produce up to 43 dpa (displacements per atom) and ~1500 appm of rhenium in tungsten components during three full power years of DEMO operation. The rate of damage production is a strong function of distance from the plasma facing surface, as shown in Fig. 1 and peak damage and rhenium production is expected in region G of the divertor armour and region F of the divertor structure (see Fig. 2). In ITER the rhenium concentration is expected to be ~1800 appm after 14 years of operation [5].

It is important to investigate the effect transmutation of tungsten to rhenium will have in conjunction with the displacement damage cascades caused by 14 MeV neutrons, due to the fact rhenium addition is known to cause embrittlement in neutron irradiated tungsten [6], and this could affect the life of tungsten components within a fusion reactor. Neutron irradiations at damage levels from 0.15 to 1.54 dpa in pure tungsten and tungsten rhenium alloys (ranging from 3 to 26% concentration of rhenium) have been conducted to investigate the effect of rhenium addition on neutron damage [6–8]. The damage mechanism has been observed to differ, depending on whether the pure tungsten transmutates to rhenium, following neutron damage, or if rhenium is already present in the alloys prior to neutron irradiation. These experiments have provided valuable information on the effect of rhenium on the neutron irradiation damage mechanism in tungsten, both as a transmutation product, and also as an alloying element prior to irradiation. However due to the nature of neutron experiments it is currently unfeasible to reach dpa levels expected in a fusion reactor like DEMO. Also due to the activity of the samples, analysis can be logistically very difficult. For this reason other, faster methods are being pursued in conjunction with neutron damage experiments to obtain more information on irradiation

* Corresponding author.
E-mail address: aneeqa.khan-3@postgrad.manchester.ac.uk (A. Khan).

http://dx.doi.org/10.1016/j.jnucmat.2016.05.003

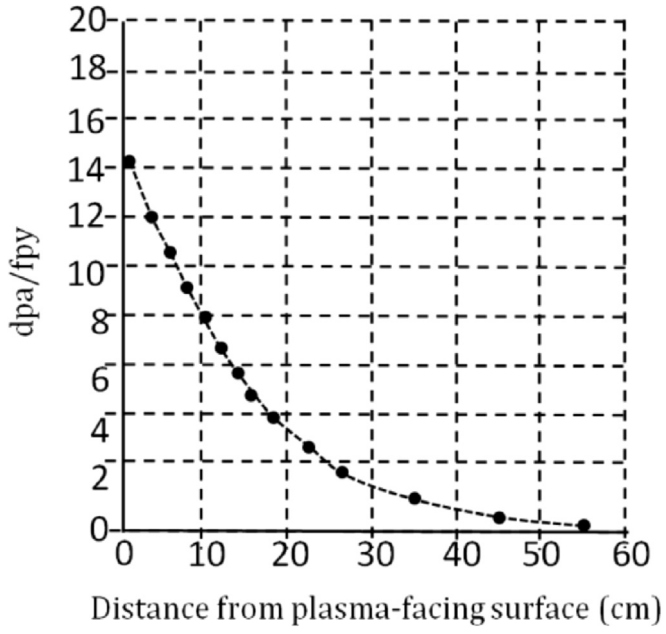

Fig. 1. dpa/fpy values for W with distance from plasma facing surface using the latest W-TENDL 2011 neutron library [22].

tungsten-rhenium matrix.

In addition to the particle damage, irradiation temperature also has an effect on changes to mechanical and microstructural properties [12], and as it is predicted that temperatures of 400 °C will be reached at the surface of the ITER outer target [1], in this experiment, the mechanical properties of as-received and annealed tungsten samples are studied following irradiation with tungsten and rhenium ions at 400 °C.

2. Materials and methods

2.1. Sample preparation

Tungsten samples were prepared from a 2 mm thick sheet of commercial purity (99.95%) tungsten supplied by Goodfellow Cambridge Ltd. The as-received sheet had a cube recrystallized texture. Samples with dimensions 1 cm × 1 cm were cut from the sheet and half of these were annealed under vacuum for 18 h at 1400 °C in order to produce a uniform microstructure. All the samples were polished to a mirror finish by firstly grinding the samples with SiC paper with decreasing grit size, then polishing with 3 and 1 μm diamond suspension, and finally polishing with colloidal alumina. The samples were subsequently cleaned ultrasonically in acetone, ethanol and deionised water. The microstructures of as received and annealed samples are shown by the

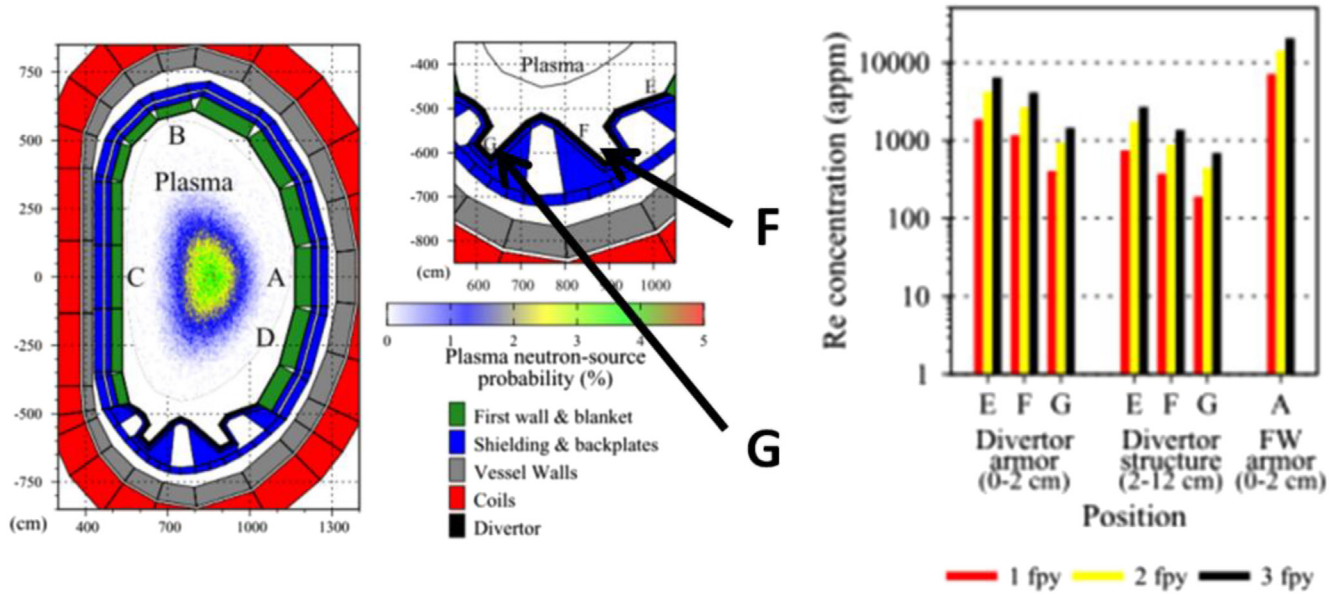

Fig. 2. Schematic of DEMO regions and variation in concentration of Re produced in pure W under neutron irradiation as a function of position and distance from the plasma facing surface in different regions of the DEMO design [5].

damage in tungsten for fusion relevant conditions.

Recently self-ion irradiations have been used to mimic the 14 MeV neutron damage expected for tungsten in a fusion reactor [9] [10]. Tungsten irradiations in alloys of W-5%Re have also been used to mimic the effects of transmutation to rhenium, while also inducing displacement damage [11]. However, as has been observed in the neutron damage experiments, the damage mechanism in pure tungsten (which transmutates to rhenium) is different to that in samples where rhenium is already present prior to irradiation. Therefore in this experiment, rhenium ions will be implanted in tungsten to simulate transmutation, at the same time as creating defects, rather than inducing damage in a pre-existing

back-scatter SEM images in Fig. 3.

These show that the grain size of the as received material is inhomogeneous, with an average grain size of approximately 1 μm, while the average grain size in the annealed samples is 21 μm (Fig. 3). Both grain sizes were calculated using the Channel 5 software package assuming a 1° misorientation.

2.2. Experimental

One set of as received and one set of annealed tungsten samples were irradiated with W and a second set with Re ions, using a tandem accelerator (National Electrostatics Corporation 5SDH) at

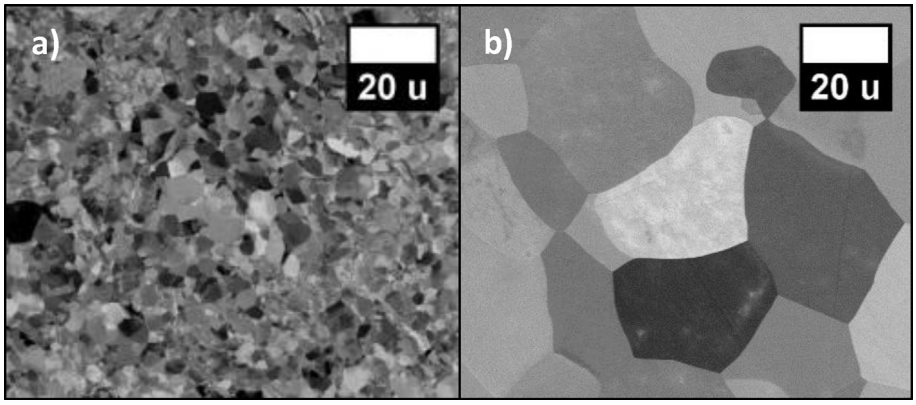

Fig. 3. SEM Back Scatter Images for a) as received and b) annealed tungsten sheet.

the Australian National University (ANU). Samples were clamped to a stainless-steel sample holder and heated to 400 °C during irradiation, which is within the operating window of the divertor in ITER [1]. The ion-irradiation conditions are summarised in Table 1.

Ion range and damage distributions were calculated using SRIM (Stopping range of ions in matter, a Monte Carlo simulation code) [13], utilising full damage calculations with 68 eV displacement energies. Multi-energy implant sequences were chosen to produce a near uniform implanted ion distribution over the depth range from 0.06 μm to 0.3 μm, as shown in Fig. 4 (i.e. 1 MeV, 2 MeV and 4 MeV ion implantations were used for each sample). The resulting rhenium concentration in this region is ~1650 appm, which is close to the 1500 appm transmutation concentration anticipated in DEMO. The peak damage (~40 dpa) achieved under these conditions is also in the range expected in DEMO.

Samples were characterised using Electron Back Scatter Diffraction (EBSD) to characterise the grain-specific irradiation damage in annealed samples, and nanoindentation to determine changes in the mechanical properties of both the as received and annealed samples.

EBSD was performed over an area of 420 by 320 μm on the annealed sample (Fig. 5), utilising a step size of 0.5–0.6 μm and accelerating voltages of 15, 20 and 30 kV. EBSD inverse pole figure (IPF) maps of the annealed W and Re irradiated samples were also produced (Figs. 6 and 7). Different voltages were used in order to study variations in ion irradiation damage close to the surface. The higher the voltage utilised, the larger the penetration depth of the back scatter electrons. The CASINO program, version 2.48 (monte CArlo Simulation of electron trajectory in sOlids) was used to determine the maximum penetration depth of back scatter electrons [14]. The software is freely available and accessible online [15].

Low load nanoindentation was performed with a Hysitron triboindenter using a Berkovich tip and was used to measure the mechanical properties of samples to depths of 200 nm. The system is capable of producing reliable results for depths as small as 50 nm.

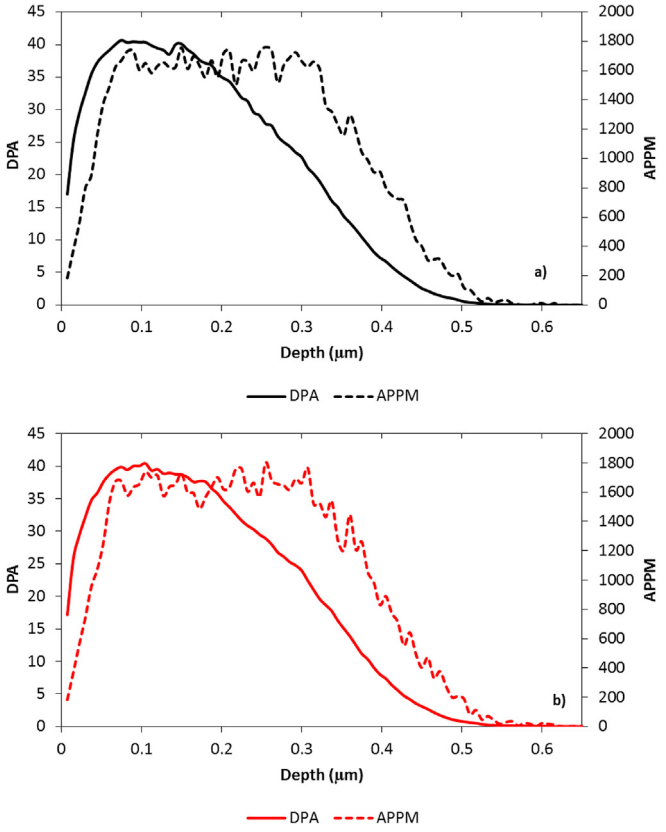

Fig. 4. Stopping range of ions in matter (SRIM) calculated profiles of displacements per atom and atomic parts per million of a) rhenium implanted in rhenium irradiated tungsten and b) tungsten implanted in tungsten irradiated tungsten at 1; 2 and 4 MeV using a 68 eV displacement value.

Table 1
W and Re ion irradiation conditions on annealed and as received targets.

Species	Energy (MeV)	Fluence (/cm^2)	Temperature (°C)	Charge state	Target current (nA)	Flux (/cm^2/s)
W	1	4.80E+14	400	1	120	1.7E+11
	2	7.00E+14	400	1	120	1.7E+11
	4	2.80E+15	400	2	120	8.3E+10
Re	1	4.80E+14	400	1	150	2.1E+11
	2	6.50E+14	400	1	500	6.9E+11
	4	2.80E+15	400	2	600	4.2E+11

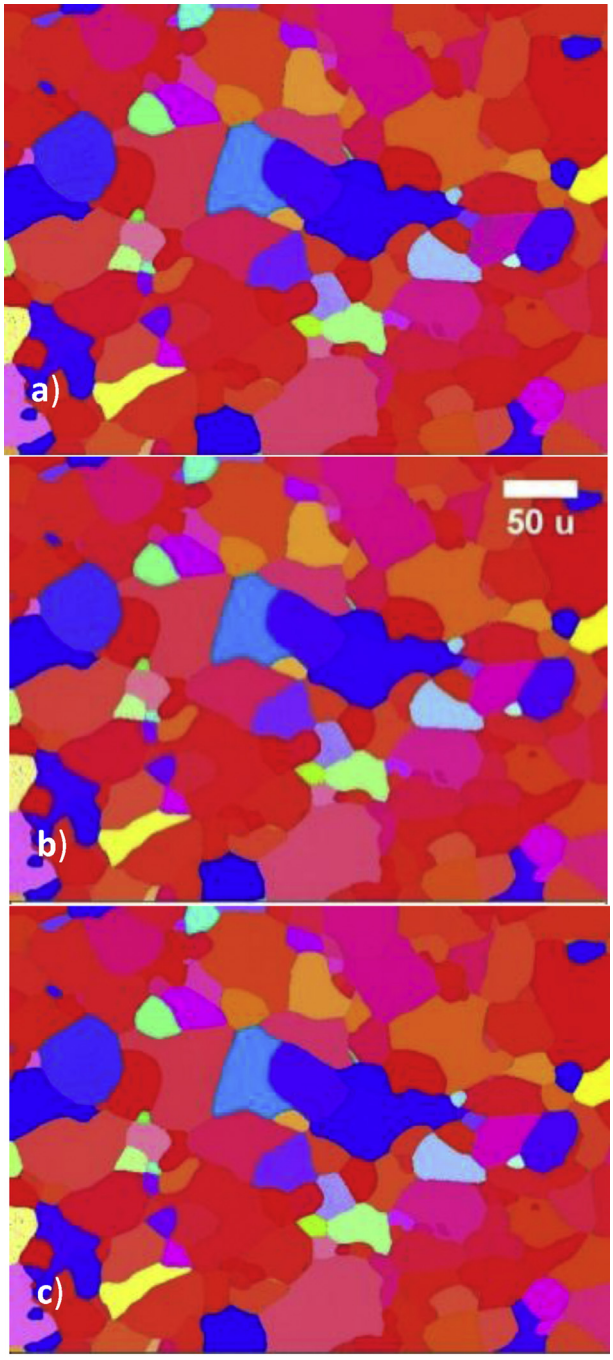

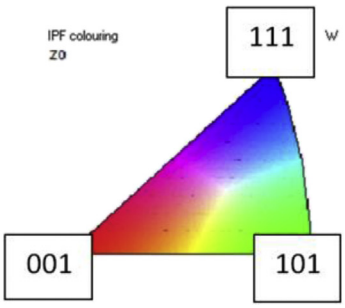

Fig. 5. Pole Figures overlaid on band contrast image at a)15 kV, b)20 kV and c) 30 kV in annealed W.

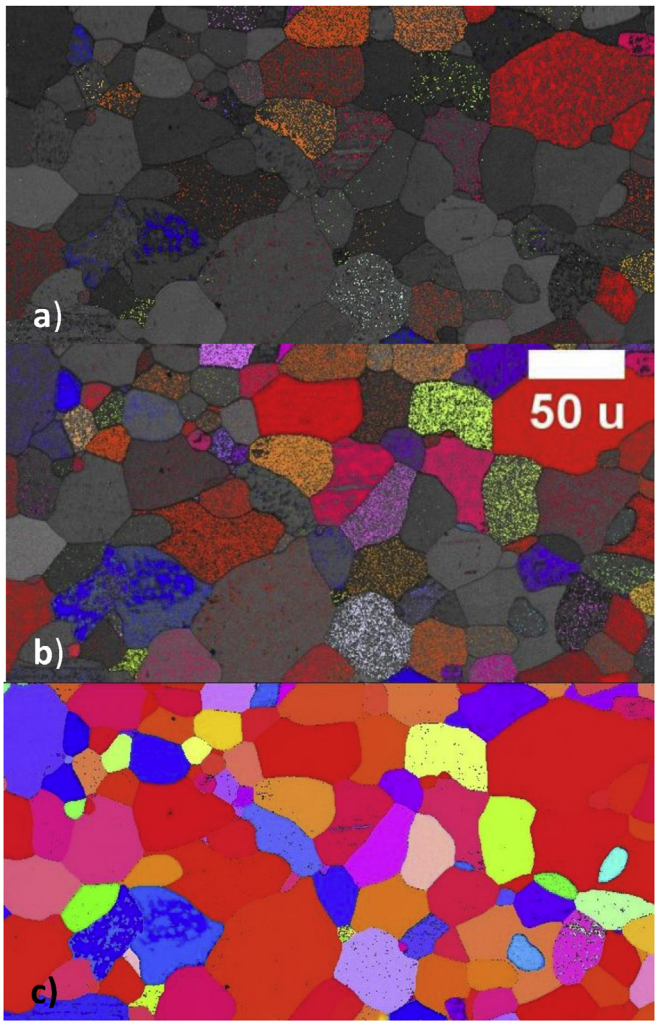

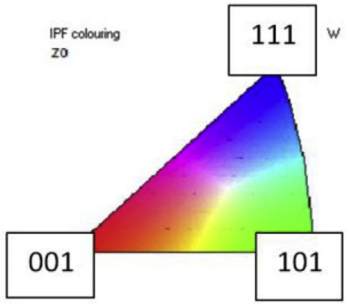

Fig. 6. Pole Figures overlaid on band contrast image at a)15 kV, b)20 kV and c) 30 kV in Re irradiated annealed W.

Variation in hardness from depths of 50–200 nm were achieved by performing measurements over an array of 150 indents (15 by 10 array, with 20 μm between each indent), ranging in depth from 50 nm to 200 nm into the sample. The indents were displacement controlled with a 5 s loading segment, followed by a 2 s hold. The same array of indents was applied to a silica standard in order to calibrate the results.

Measurements of modulus and hardness were calculated for each indent from the unload portion of each load/unload curve. Supplied software was used to calculate the reduced modulus E_r, which was converted to actual modulus using Equation (1) [16].

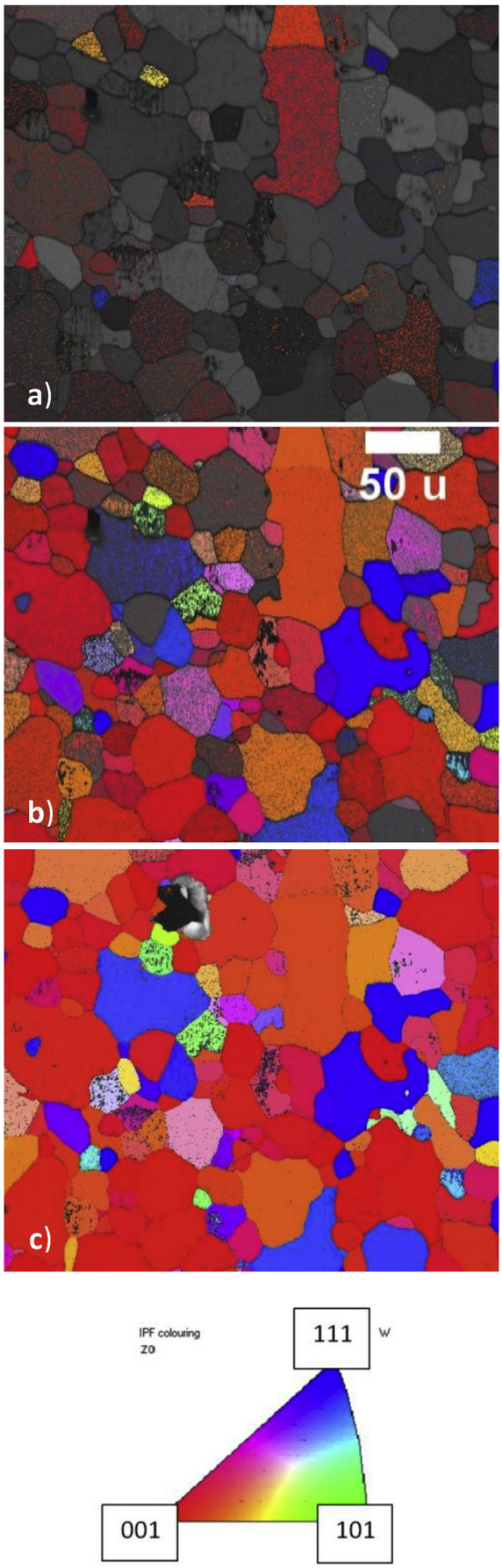

$$\frac{1}{E_r} = \frac{(1-\nu^2)}{E} + \frac{(1-\nu_i^2)}{E_i} \quad (1)$$

where E_i and ν_i are the modulus and Poisson's ratio of the indenter material and ν is the Poisson's ratio of the material being indented. The indenter tip is made of diamond, where E_i is equal to 1141 GPa and ν_i is equal to 0.07 [17]. The Poisson's ratio of tungsten was assumed to be 0.28.

3. Results and discussion

3.1. Quality of EBSD results

First we consider the EBSD results for the annealed, non-irradiated samples, as shown in Fig. 8. Here, the hit rate (the percentage of Kikuchi patterns that have successfully been indexed) for all samples was above 99% and the Inverse Pole Figure (IPF) maps (Fig. 5) were completely indexed across all grains. For the tungsten and rhenium irradiated samples the situation was quite different. In both cases the hit rate was above 94% for 30 keV electrons. However, at 20 kV, significant degradation in the images and pole figures was observed (Figs. 6 and 7). At 15 kV the hit rate for both samples was further reduced to less than 10% in both cases. It should be noted that SRIM calculations indicate a sputtering rate of ~12 atoms/ion, which for the fluences employed corresponds to the removal of <2 nm of W from the surface, therefore even allowing for the orientation dependence of the sputtering rate, no surface roughening is expected. This reduction in hit rate is therefore due to the fact that certain grain orientations are not indexing, and indeed no Kikuchi patterns are observed for these grains at the lower voltages. This can be correlated with the penetration depth of the back scatter electrons using the CASINO code [15], as shown in Fig. 9. Such analysis shows that 95% of the back scatter electron signal emerges from 87 nm for 15 keV electrons, 138 nm for 20 keV electrons, and 264 nm for 30 keV electrons (see Fig. 10). This suggests that closer to the surface of the sample; at depths up to 138 nm below the surface of the sample, the irradiation damage is highly orientation specific. This lies within the peak damage region of the samples and means that irradiation damage is most likely to be grain orientation dependent. A good band contrast image is obtained regardless of accelerating voltage even though the individual 'pixels' are not indexed. This is because significant signal was still generated from the heavily damaged region. There was no apparent change in grain size or texture for irradiated samples.

3.2. Change of mechanical properties

The mechanical properties of annealed samples before and after irradiation are summarised in Fig. 11, and those for as-received samples before and after irradiation are summarised in Fig. 12. Comparison of Figs. 11a) and 12a) shows that the modulus of both annealed and as received samples is unchanged by irradiation and is approximately constant over the whole depth of measurement. The modulus of all samples is within 5.5% of the expected modulus for tungsten of 410 GPa [2], with the exception of the non-irradiated as-received sample which showed a slightly greater deviation of 8.9%. This is greater than the expected tolerance of the measurement system, which is ±5%.

Although the modulus is constant over depths of 50–200 nm,

Fig. 7. Pole Figures overlaid on band contrast image at a)15 kV, b)20 kV and c) 30 kV in W irradiated annealed W.

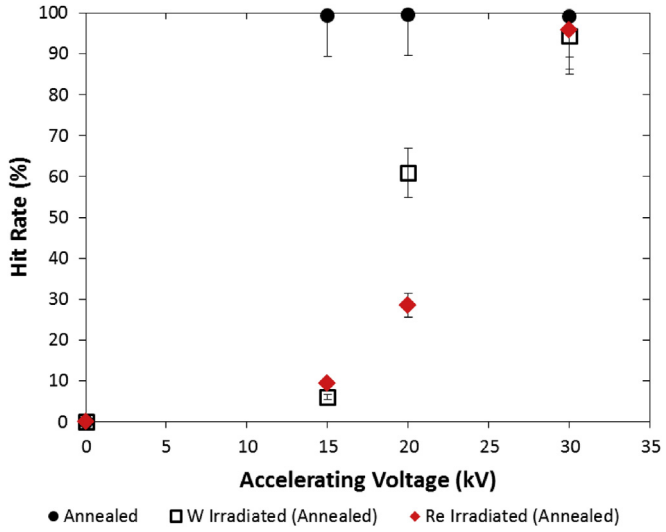

Fig. 8. Relationship between Accelerating Voltage and Hit Rate of EBSD map in annealed and irradiated annealed irradiated samples.

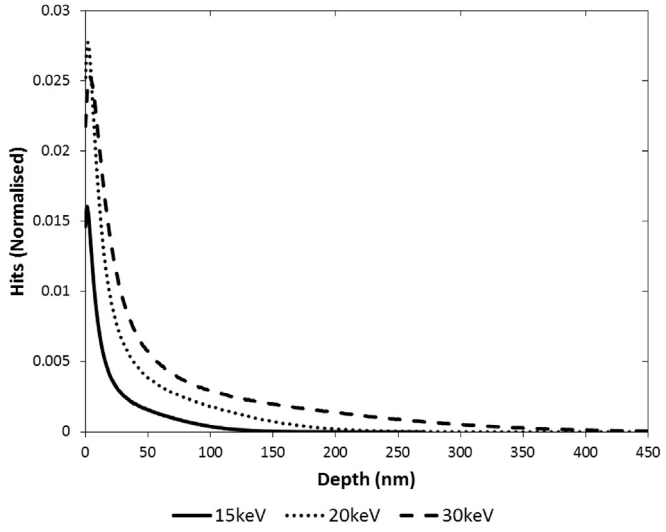

Fig. 9. Normalised hits of backscattered electrons vs penetration depth at a) 15 keV, b) 20 keV and c) 30 keV calculated using CASINO.

there is a clear decrease in hardness with increasing indent depth (Figs. 11b) and 12b)). This is explained by the Nix Gao relationship. The Nix and Gao model states that square of the hardness is directly proportional to the reciprocal of the depth of the indenter into a polycrystalline sample when the measurement is no longer limited by 'tip effects' (tip blunting or deformities at low loads) [18]. The advantage of this high resolution technique means that these values are directly proportional, even at displacements as small as 50 nm, as illustrated in Figs. 11c) and 12c)).

From Fig. 11b)) it can be observed that there is an approximate 23% increase in hardness for the rhenium and tungsten irradiated annealed samples. This increase is almost the same, regardless of the implanted ion species. For the as received samples, the actual hardness is on average 0.4 GPa higher, but a similar trend is still observed, as shown in Fig. 12b). However, the increase in hardness is only ~13% for the rhenium irradiated and tungsten irradiated as-received samples. In the case of W irradiations, the implanted ions become part of the matrix, indistinguishable from the host atoms.

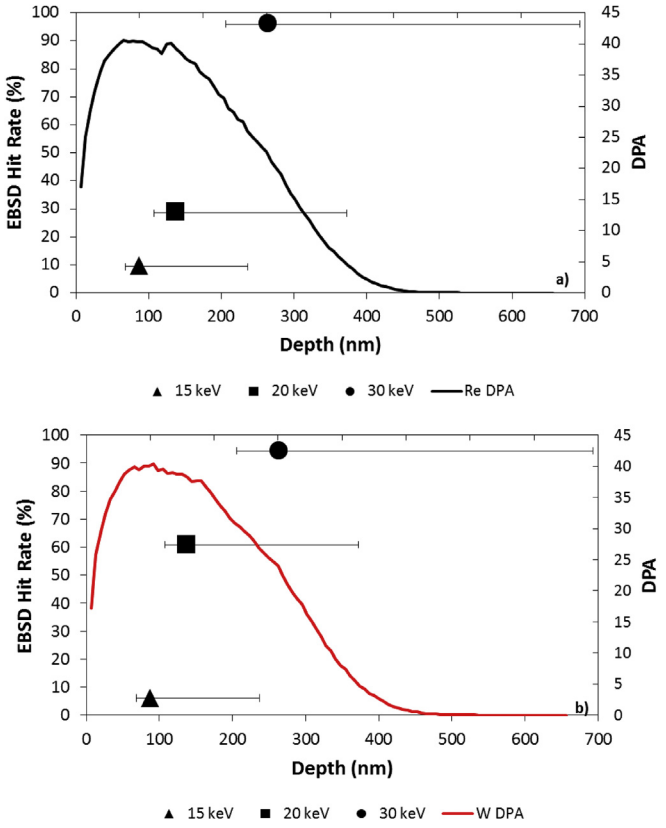

Fig. 10. Overlay of EBSD hit rate against 95% of CASINO calculated penetration depth, with error bars highlighting 100% and 90% penetration depth for 15, 20 and 30 keV over DPA damage profile of a) rhenium irradiated tungsten and b) tungsten irradiated tungsten.

The Re will also substitute for W, forming a substitutional solid solution as we are below the solubility limit of 30 at.% [19]. This indicates that while simultaneously implanting rhenium at concentrations of approximately 1600appm, and inducing cascade damage of approximately 40 dpa the substitution of rhenium atoms into the tungsten matrix, rather than tungsten atoms has a negligible effect on hardness and modulus changes. It is the displacements created, rather than the introduction of a new element into the matrix that is driving the damage mechanism. This is consistent with the fact that the damage from the tungsten and rhenium ion irradiations is comparable due to the fact the mass number of tungsten is 184 and that of rhenium is 187. The greater hardness increase in the annealed samples in comparison to the as-received is consistent with other literature, where W was irradiated with Fe ions, and is due to the fact the grain boundary area (a sink site) in the annealed samples is smaller than in the as-received [20].

If we compare our results to those of Armstrong et al., where irradiations were carried out in pure W and W-5%Re at temperatures of ~300 °C, utilising an energy of 2 MeV to achieve a damage level of 33 dpa where there was a 12% increase in hardness in tungsten (50–500 μm grain size) and a 45% increase in hardness of the W-5%Re (10–100 μm grain size). It is interesting that at lower temperatures and a slightly lower dpa level than the data presented in this paper the hardness increase observed in W-5%Re was so large. If we compare to our rhenium irradiated annealed material, with average grain size of 21 μm, which is comparable to the grain size of the W-5%Re Armstrong et al. utilised, the hardness increase is less than half of that observed by Armstong et al., suggesting that the presence of rhenium is dominating the damage mechanism,

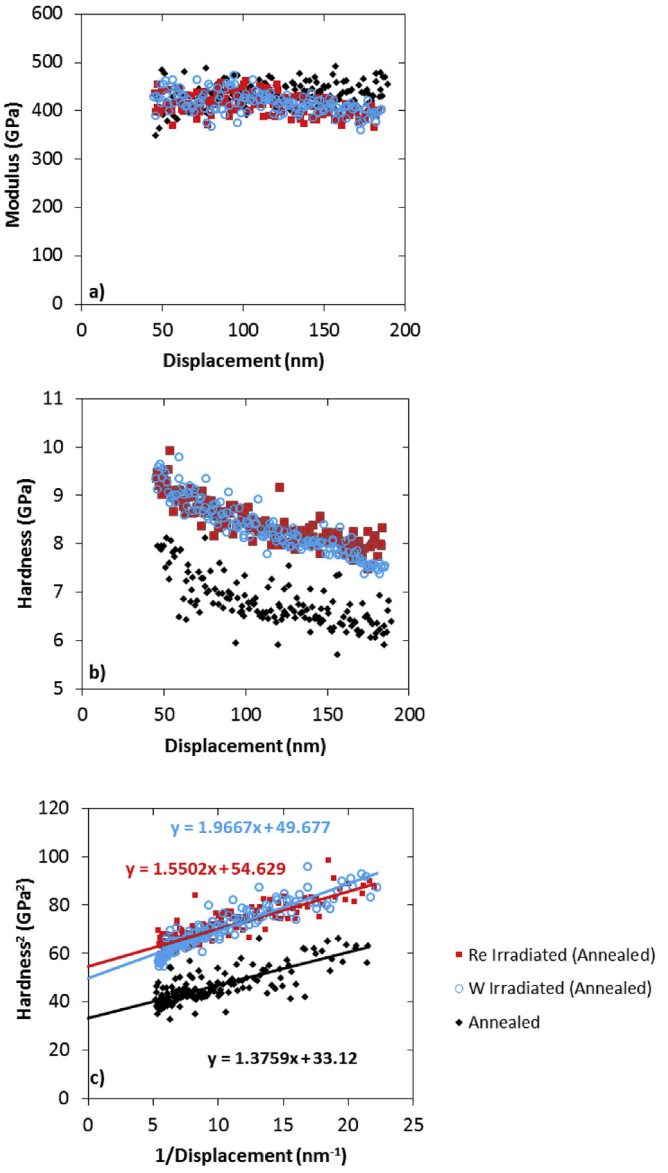

Fig. 11. Measurement of a) actual modulus against displacement, b) hardness against displacement and c) demonstration of the Nix Gao relationship – Hardness^2 against reciprocal of displacement sample for non-irradiated and W and Re irradiated annealed samples.

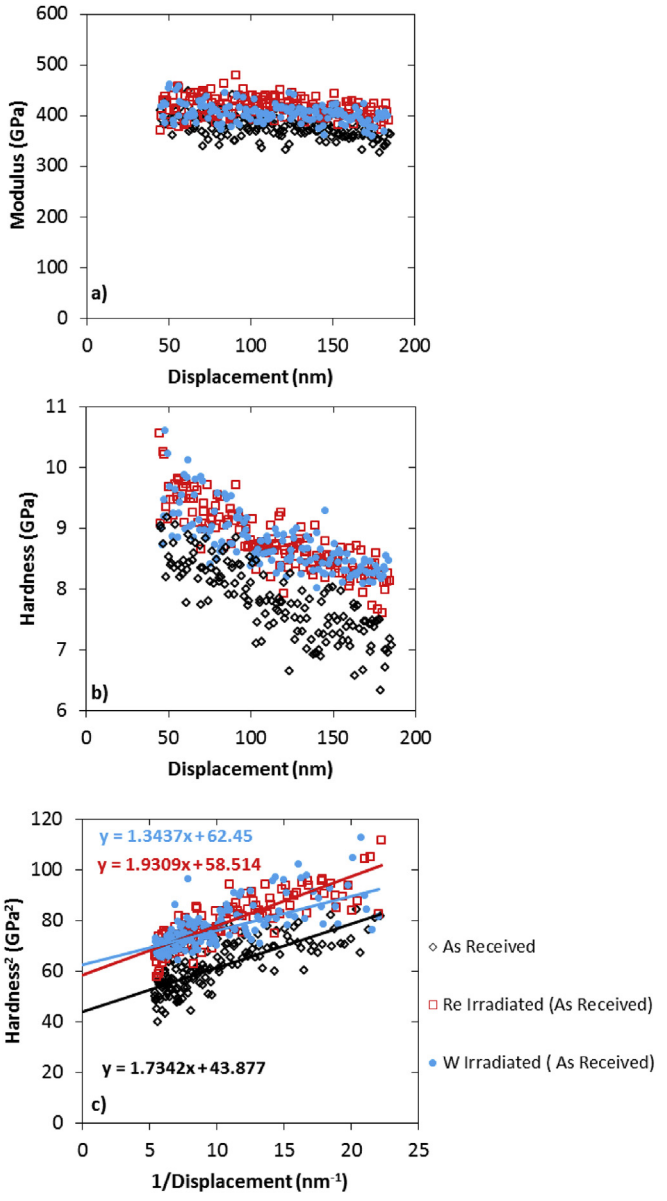

Fig. 12. Measurement of a) actual modulus against displacement, b) hardness against displacement and c) demonstration of the Nix Gao relationship – Hardness^2 against reciprocal of displacement sample for non-irradiated and W and Re irradiated as received samples.

which is clearly not the case with the lower concentrations we utilised. The hardness increase observed in the as received tungsten in this experiment are comparable to that observed by Armstrong et al. However the annealed tungsten in this study showed double this increase in hardness, which considering the smaller grain size, suggests that the increase in temperature and increase in dpa used in this study are resulting in a greater increase in hardness [11]. This corresponds to the fact that at higher temperatures, displacement energies are lower [21], resulting in increased damage. The results presented in this paper are only for irradiations at 400 °C.

4. Conclusions

The effect of radiation damage and implanted rhenium on the hardness and modulus of as received and annealed tungsten samples was investigated by irradiating them with both tungsten ions and rhenium ions at a temperature of 400 °C. It was found that at peak damage levels of around 40 dpa the originally annealed samples underwent a 23% increase in hardness, while as received samples showed a 13% increase. The effect of rhenium irradiation was found to be indistinguishable from that of tungsten irradiation for peak rhenium concentrations up to 1600 appm. For annealed samples, it was further observed that both kinds of ion irradiation caused significant surface damage to the samples, which was grain orientation dependant. This was confirmed by the EBSD image degradation with decreasing electron accelerating voltage, which corresponds to a decreasing penetration depth as calculated using CASINO software. The fact that image degradation varied with grain orientation suggests that the ion irradiation damage is orientation dependant.

Acknowledgements

We acknowledge access to NCRIS facilities (ANFF and the Heavy Ion Accelerator Capability) at the Australian National University. This work was supported by the Engineering and Physical Sciences Research Council [EP/K504178/1]. Thanks are also given to Andy Wallwork for his help with the annealing of the samples and to Marc Schmidt for his help with EBSD. The author also gratefully acknowledges the useful conversations with Michael Faulkner.

References

[1] R.A. Pitts, S. Carpentier, F. Escourbiac, T. Hirai, V. Komarov, S. Lisgo, A.S. Kukushkin, A. Loarte, M. Merola, A. Sashala Naik, R. Mitteau, M. Sugihara, B. Bazylev, P.C. Stangeby, J. Nucl. Mater 438 (2013) S48.
[2] Materials: Tungsten, PLANSEE, 2013 [Online]. Available, http://www.plansee.com/en/Materials-Tungsten-403.htm [Accessed: 02-Jul-2013].
[3] Y. Ueda, H.T. Lee, N. Ohno, S. Kajita, A. Kimura, R. Kasada, T. Nagasaka, Y. Hatano, A. Hasegawa, H. Kurishita, Y. Oya, Phys. Scr. T145 (2011) 014029.
[4] M. Rieth, J.L. Boutard, S.L. Dudarev, T. Ahlgren, S. Antusch, N. Baluc, M.-F. Barthe, C.S. Becquart, L. Ciupinski, J.B. Correia, C. Domain, J. Fikar, E. Fortuna, C.-C. Fu, E. Gaganidze, T.L. Galán, C. García-Rosales, B. Gludovatz, H. Greuner, K. Heinola, N. Holstein, N. Juslin, F. Koch, W. Krauss, K.J. Kurzydlowski, J. Linke, C. Linsmeier, N. Luzginova, H. Maier, M.S. Martínez, J.M. Missiaen, M. Muhammed, A. Muñoz, M. Muzyk, K. Nordlund, D. Nguyen-Manh, P. Norajitra, J. Opschoor, G. Pintsuk, R. Pippan, G. Ritz, L. Romaner, D. Rupp, R. Schäublin, J. Schlosser, I. Uytdenhouwen, J.G. van der Laan, L. Veleva, L. Ventelon, S. Wahlberg, F. Willaime, S. Wurster, M.A. Yar, J. Nucl. Mater 417 (2011) 463.
[5] M.R. Gilbert, J.-C. Sublet, Nucl. Fusion 51 (2011) 43005.
[6] T. Tanno, A. Hasegawa, J.-C. He, M. Fujiwara, S. Nogami, M. Satou, T. Shishido, K. Abe, Mater. Trans. 48 (2007) 2399.
[7] A. Hasegawa, T. Tanno, S. Nogami, M. Satou, J. Nucl. Mater 417 (2011) 491.
[8] M. Fukuda, K. Yabuuchi, S. Nogami, A. Hasegawa, T. Tanaka, J. Nucl. Mater 455 (2014) 460.
[9] D.E.J. Armstrong, A.J. Wilkinson, S.G. Roberts, Phys. Scr. T145 (2011) 14076.
[10] J. Gibson, D. Armstrong, S. Roberts, Phys. Scr. T159 (2014) 014056.
[11] D.E.J. Armstrong, X. Yi, E.A. Marquis, S.G. Roberts, J. Nucl. Mater 432 (2013) 428.
[12] C.D. Hardie, C.A. Williams, S. Xu, S.G. Roberts, J. Nucl. Mater 439 (2013) 33.
[13] J.F. Ziegler, J.P. Biersack, U. Littmark, The Stopping and Range of Ions in Solids, Pergamon, New York, 1985.
[14] D. Drouin, A.R. Couture, D. Joly, X. Tastet, V. Aimez, R. Gauvin, Scanning 29 (2007) 92.
[15] Downloads, Université de Sherbrooke, 2016 [Online]. Available, http://www.gel.usherbrooke.ca/casino/download2.html [Accessed: 14-Jan-2016].
[16] G.M. Pharr, W.C. Oliver, F.R. Brotzen, J. Mater. Res. 7 (2011) 613.
[17] G. Simmons, H. Wang, Single Crystal Elastic Constants and Calculated Elastic Properties: A Handbook, MIT Press, Cambridge, MA, 1971.
[18] W.D. Nix, H.J. Gao, J. Mech. Phys. Solids 46 (1998) 411.
[19] M. Ekman, K. Persson, G. Grimvall, J. Nucl. Mater 278 (2000) 273.
[20] Z.X. Zhang, D.S. Chen, W.T. Han, A. Kimura, Fusion Eng. Des. 98–99 (2015) 2103.
[21] K. Russell, Prog. Mater. Sci. 28 (1984) 229.
[22] M.R. Gilbert, S.L. Dudarev, D. Nguyen-Manh, S. Zheng, L.W. Packer, J.-C. Sublet, J. Nucl. Mater. (2013) 1.